Chapter 1
Numerical calculation of interior transmission eigenvalues with mixed boundary conditions

A. Kleefeld and J. Liu

Abstract Interior transmission eigenvalue problems for the Helmholtz equation play an important role in inverse wave scattering. Some distribution properties of those eigenvalues in the complex plane are reviewed. Further, a new scattering model for the interior transmission eigenvalue problem with mixed boundary conditions is described and an efficient algorithm for computing the interior transmission eigenvalues is proposed. Finally, extensive numerical results for a variety of two-dimensional scatterers are presented to show the validity of the proposed scheme.

1.1 Introduction

A transmission eigenvalue problem is a non-classical boundary value problem for a specified differential operator which acts on a pair of functions $(u(x),v(x))$ in some given open and bounded domain D, where the functions $u(x)$ and $v(x)$ are coupled on the boundary $\partial D=\Gamma$. The exterior normal on Γ is denoted by ν.

A typical example arising in acoustic wave scattering is the (classical) interior transmission eigenvalue problem with specified refraction index $n(x)\in L^\infty(D)$ satisfying $\mathrm{Re}\{n(x)\}>0$ and $\mathrm{Im}\{n(x)\}\geq 0$. It is given by

$$\begin{cases} \Delta u+k^2u=0\,, & x\in D\,,\\ \Delta v+k^2n(x)v=0\,, & x\in D\,,\\ u=v\,, \quad \frac{\partial u}{\partial \nu}=\frac{\partial u}{\partial \nu}\,, & x\in\Gamma\,, \end{cases} \tag{1.1}$$

A. Kleefeld
Forschungszentrum Jülich GmbH, Jülich Supercomputing Centre, 52425 Jülich, Germany,
e-mail: a.kleefeld@fz-juelich.de

J. Liu
School of Mathematics/Seu-Yau Center, Southeast University, Nanjing, China,
e-mail: jjliu@seu.edu.cn

for which one tries to find $k \in \mathbb{C}\backslash\{0\}$ such that there exists non-trivial solutions $(u,v) \in L^2(D) \times L^2(D)$ and $u - v \in H_0^2(D)$. These values k are called (classical) interior transmission eigenvalues (ITEs).

Originally, the distribution properties of the eigenvalues such as discreteness and their asymptotic behavior have been studied in detail in order to determine characteristics of media [CoMo87, CoMo88, Ki86] as well as the existence [CaGiHa10]. These properties are not trivial to derive due to the fact that the underlying eigenvalue problem is neither elliptic nor self-adjoint. Hence, it cannot be investigated by using standard spectral theory for differential operators. Hence, this interior transmission problem is of interest to researchers working on non-standard spectral problems. Additionally, researchers are interested in finding incident waves that do not scatter which is closely related to the interior eigenvalue problem (1.1) (see for example [GiPa13]).

Reconstruction algorithms for inverse scattering problems are for example the linear sampling method and the factorization method [CaCo06, KiGr08] which are not justified theoretically for wave numbers that are ITEs. Hence, researchers started to compute such exceptional values. It has been shown that ITEs can be determined from scattered data or far-field data [CaCoHa10]. Since then, a variety of new methods such as FEM [LiHuLiLi15, Su11], BEM [Kl13, Kl15] and the inside-outside-duality method [KiLe13] have appeared (see [KlPi18] for a recent and detailed overview as well as the MFS method). However, the numerical calculation of those is still an on-going and challenging research topic especially the calculation of complex-valued ITEs whose existence is still open for general scatterer.

However, motivated by a more general physical configuration, the transmission eigenvalue problems may be of a more complicated form. We consider the situation where an inhomogeneous obstacle D is located in a perfect conducting substrate D_2 with the boundary $\Gamma_2 \subset \Gamma$, while the remaining part of the boundary $\Gamma_1 = \Gamma \setminus \Gamma_2$ contacts with the surface of background dielectric medium D_1. See Fig. 1.1 for an illustration of the situation. Then the following interior transmission problem with

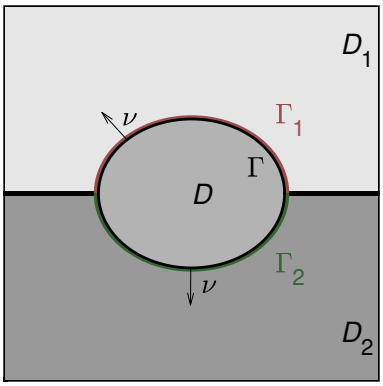

Fig. 1.1 Exemplary setup of the physical configuration.

mixed boundary condition arises (see also [YaMo14] and [LiLi16]):

$$\begin{cases} \Delta u + k^2 u = 0\,, & x \in D\,, \\ \Delta v + k^2 n v = 0\,, & x \in D\,, \\ u = v\,, \quad \frac{\partial u}{\partial \nu} = \frac{\partial v}{\partial \nu}\,, & x \in \Gamma_1\,, \text{ (transmission condition)} \\ u = v = 0\,, & x \in \Gamma_2\,, \text{ (hom. Dirichlet condition)} \end{cases} \tag{1.2}$$

with $\Gamma = \Gamma_1 \cup \Gamma_2$ assuming $\Gamma_1 \neq \emptyset$ and $\Gamma_2 \neq \emptyset$. Here, $n(x) \neq 1$ is the real-valued index of refraction. Although the distributions and the discreteness properties have been analyzed in [LiLi16] for general complex-valued $n(x)$, the efficient numerical calculation of mixed interior transmission eigenvalues (MITEs) is still absent. This is mainly due to the presence of the mixed boundary condition on Γ which causes extra difficulties for the construction of suitable basis functions that are needed in the finite element method.

But the boundary integral equation method is a powerful tool for solving boundary value problems of partial differential equations (PDEs), especially when the problem is homogeneous and the fundamental solution to the corresponding PDE can be represented explicitly. The main advantage of solving boundary value problems by this scheme is, by representing the solution in potential form, the solution can be essentially converted into the task of finding a density function defined on the boundary of the domain, and consequently the amount of computations can be dramatically decreased (see [Kl12a]). By this motivation, we propose to solve the mixed transmission eigenvalue problem (1.2) with constant refraction index $n(x) \equiv n$ (constant) in $D \subset \mathbb{R}^2$ by the boundary integral equation method since the fundamental solution can be given explicitly in analytic form.

Contribution within this chapter

First, a short summary for the existence and discreteness for the real-valued index of refraction not equal to one is given in Section 1.2. Although the results are a special case of [LiLi16], the sufficient conditions on the index of refraction as well as the estimates of the lower bound of positive eigenvalues can be stated more clearly. Second, a derivation of a system of boundary integral equations to solve the mixed interior transmission problem including its approximation via boundary element collocation method leading to a non-linear eigenvalue problem is given in Section 1.3. Lastly, extensive numerical results for the computations of mixed interior transmission eigenvalues are presented for the first time for various scatterers in two dimensions in Section 1.4. In addition, the corresponding eigenfunctions are shown as well. A short summary and conclusion is given in Section 1.5. Finally, for the special case of the unit square an alternative method is given in the Appendix to find mixed interior transmission eigenvalues.

1.2 A review on some theoretical results

To consider the numerical computations for the transmission eigenvalues of (1.2), we first need the distribution properties of the eigenvalues. Although the properties of the eigenvalues with classical boundary conditions have been thoroughly studied, the theoretical results for eigenvalues using mixed boundary conditions as studied here are still rare (see [LiLi16]). Since our numerical scheme for computing the eigenvalues by boundary integral equations is established for the constant index of refraction $n(x) \equiv n_0$ in $\overline{D}$ for $0 < n_0 < 1$ or $n_0 > 1$, some existing results for the distributions of eigenvalues under the assumption either $n(x) \in (0,1)$ or $n(x) > 1$ are applicable.

In this section, we give these theoretical properties of the transmission eigenvalues for $n(x) \in C(D)$ with either positive lower point $n_- > 1$ or positive upper bound $n_+ < 1$, which means that there are no zero points of $n(x) - 1$ in $\overline{D}$. These results can be considered as special cases established in [LiLi16] for both complex-valued refraction index $n(x)$ and complex-valued background medium. However, in our case with real-valued index of refraction $n(x)$, the corresponding results can be much more simplified. To state the results clearly, we introduce the Sobolev space

$$\begin{aligned}\tilde{H}_{0,1}(D) = \big\{ & w \in L^2(D), \quad \nabla w \in (L^2(D))^2, \quad \Delta w \in L^2(D), \\ & w = 0 \text{ on } \Gamma, \quad \nu \cdot \nabla w = 0 \text{ on } \Gamma_1 \big\},\end{aligned}$$

with scalar product

$$\langle u, v \rangle_{\tilde{H}_{0,1}(D)} = (u,v)_{L^2(D)} + (\nabla u, \nabla v)_{L^2(D)} + (\Delta u, \Delta v)_{L^2(D)}$$

for two complex-valued functions u and v from $\tilde{H}_{0,1}(D)$. Then the transmission eigenvalue problem (1.2) can be restated as: Find $k \in \mathbb{C} \backslash \{0\}$ such that there exists a non-zero pair $(u,v) \in (L^2(D))^2$ satisfying $v - u \in \tilde{H}_{0,1}(D)$ and

$$\begin{cases} \Delta u + k^2 u = 0, & x \in D, \\ \Delta v + k^2 n v = 0, & x \in D, \\ u = v = 0, & x \in \Gamma_2. \text{ (hom. Dirichlet condition)} \end{cases}$$

Note that the transmission conditions in (1.2) have been incorporated in the requirement $v - u \in \tilde{H}_{0,1}(D)$. In the case $\Gamma_2 = \emptyset$, it is well-known based on the analytic Fredholm theorem that the set of ITEs is at most discrete with $+\infty$ as the only possible accumulation point. We will prove that such a property is also true for our problem (1.2) with mixed boundary condition. Therefore, define $z = v - u$ and $n_c(x) = n(x) - 1 \neq 0$ in $\overline{D}$. Since $z \in \tilde{H}_{0,1}(D)$ fulfills

$$\Delta z + k^2 z = -k^2 v n_c, \tag{1.3}$$

by deleting v, $z(x)$ satisfies the following differential equation of fourth order

$$\left(\Delta + k^2 n(x)\right) \frac{1}{n_c(x)} \left(\Delta + k^2\right) z = 0\,, \quad x \in D\,. \tag{1.4}$$

Using (1.3) and the boundary condition $v|_{\Gamma_2} = 0$, we have

$$\frac{1}{n_c(x)} \left(\Delta + k^2\right) z = 0 \qquad \text{on } \Gamma_2\,.$$

With $z|_{\Gamma_2} = v|_{\Gamma_2} - u|_{\Gamma_2} = 0$ it can be further simplified to

$$\frac{1}{n_c(x)} \Delta z = 0 \qquad \text{on } \Gamma_2\,,$$

Therefore, we conclude that the transmission eigenvalues $k \in \mathbb{C}\backslash\{0\}$ are those values such that there exists some non-trivial solution $z \in \tilde{H}_{0,1}(D)$ satisfying

$$\begin{cases} \left(\Delta + k^2 n(x)\right) \frac{1}{n_c(x)} \left(\Delta + k^2\right) z = 0\,, & x \in D\,, \\ z = 0\,, & x \in \Gamma = \Gamma_1 \cup \Gamma_2\,, \\ \frac{1}{n_c(x)} \Delta z = 0\,, & x \in \Gamma_2\,, \\ \frac{\partial z}{\partial \nu} = 0\,, & x \in \Gamma_1\,. \end{cases} \tag{1.5}$$

The distributions of the transmission eigenvalues can be analyzed in terms of (1.5). To this end, we need the following estimate for $u \in \tilde{H}_{0,1}(D)$ (see [YaMo14]), which can be considered as a generalization of the Poincaré inequality, and can be applied to estimate the lower bound of real-valued eigenvalues in order to qualify the numerical results.

Lemma 1. *For any $w \in \tilde{H}_{0,1}(D)$, we obtain the estimate*

$$\|\nabla w\|^2_{L^2(D)} \leq \frac{1}{\lambda(D)} \|\Delta w\|^2_{L^2(D)}\,.$$

Here, $\lambda(D)$ denotes the first eigenvalue of the buckled plate eigenvalue problem given by:

$$\begin{cases} -\Delta^2 w = \lambda \Delta w\,, & \text{in } D\,, \\ w = 0\,, & \text{on } \Gamma = \Gamma_1 \cup \Gamma_2\,, \\ \nu \cdot \nabla w = 0\,, & \text{on } \Gamma_1\,, \\ \Delta w = 0\,, & \text{on } \Gamma_2\,. \end{cases}$$

For a real-valued index of refraction $0 < n(x) \neq 1$ in $\overline{D}$, there exists two constant $n_- > 0$ and $n_+ > 0$ such that

$$\begin{aligned} n_+ \geq n(x) \geq n_- > 1\,, \qquad & \text{if } \; n(x)|_{\overline{D}} > 1\,, \\ 1 > n_+ \geq n(x) \geq n_- > 0\,, \qquad & \text{if } \; n(x)|_{\overline{D}} < 1\,, \end{aligned}$$

which ensures

$$\frac{1}{|n(x)-1|} \geq \alpha > 0\,, \quad x \in \overline{D}$$

for some small constant $\alpha > 0$. Based on Lemma 1, the following results state the distribution properties of the mixed interior transmission eigenvalues (MITEs).

Theorem 1. *For a real-valued index of refraction $0 < n(x) \neq 1$ in $\overline{D}$, we assume that*

$$\begin{aligned} 0 < \frac{1}{n_- - 1} < 1\,, &\qquad \text{if } n(x)|_{\overline{D}} > 1\,, \\ 0 < \frac{n_+}{1-n_+} < 1\,, &\qquad \text{if } n(x)|_{\overline{D}} < 1\,. \end{aligned} \tag{1.6}$$

Then the set of MITEs is at most discrete and does not accumulate at zero and all the real-valued MITEs (if they exist) are such that

$$k^2 \geq \begin{cases} \lambda(D)\frac{n_- - 2}{n_-(n_- - 1)}\,, & \text{if } n(x)|_{\overline{D}} > 1\,, \\ \lambda(D)\frac{1-2n_+}{1-n_+}\,, & \text{if } n(x)|_{\overline{D}} < 1\,, \end{cases}$$

where $\lambda(D)$ is the first eigenvalue of (1.4).

This result is just a special case of [LiLi16, Theorem 3.3] since we have

$$\begin{aligned} 0 < \frac{1}{|n(x)-1|} = \frac{1}{n(x)-1} \leq \frac{1}{n_- - 1} = \alpha\,, &\quad \text{if } n(x)|_{\overline{D}} > 1\,, \\ 0 < \frac{1}{|n(x)-1|} = \frac{1}{1-n(x)} \leq \frac{1}{1-n_+} = \alpha\,, &\quad \text{if } n(x)|_{\overline{D}} < 1\,. \end{aligned}$$

Therefore, we omit the details for the proof. As for the existence of mixed interior transmission eigenvalues, [LiLi16, Theorem 3.7] leads to the following result.

Theorem 2. *If (1.6) is replaced by the assumptions*

$$\begin{aligned} 0 < \frac{1}{n_- - 1} < \frac{1}{8}\,, &\qquad \text{if } n(x)|_{\overline{D}} > 1\,, \\ 0 < \frac{n_+}{1-n_+} < \frac{1}{8}\,, &\qquad \text{if } n(x)|_{\overline{D}} < 1\,, \end{aligned} \tag{1.7}$$

then there exists an infinite number of transmission eigenvalues with $+\infty$ as the only possible accumulation point.

Remark 1. The assumption (1.6) or (1.7) can be explained easily. Roughly speaking, in the case $n(x)|_{\overline{D}} \neq 1$, if the values of $n(x)$ are far away from the background index $n_0(x) \equiv 1$, then there always exist discrete transmission eigenvalues (but not necessarily being real-valued) with $+\infty$ as the only possible accumulation point. In Theorem 1, we need $n(x) > n_- > 2$ for $n(x) > 1$ and $n(x) < n_+ < 1/2$ for $0 < n(x) < 1$.

This condition is strengthened in Theorem 2 as $n(x) > n_- > 9$ for $n(x) > 1$ and $n(x) < n_+ < 1/9$ for $0 < n(x) < 1$.

Based on the theoretical results for the distributions of transmission eigenvalues for a real-valued index of refraction $n(x) \neq 1$, we consider the numerical calculation of mixed interior transmission eigenvalues for $n(x)$ being constant in $\overline{D}$ by focusing on the boundary integral equation method in the next section.

1.3 System of boundary integral equations and its approximation

In this section, we derive a 4×4 system of boundary integral equations to solve the interior transmission problem with mixed boundary conditions.

Denote by $\Phi_k(x,y) = \mathrm{i}H_0^{(1)}(k|x-y|)/4, x \neq y$ the fundamental solution of the two-dimensional Helmholtz equation with wave number k. The single- and double-layer potentials for the Helmholtz equation over the surface Γ are given for $x \notin \Gamma$ by

$$\begin{aligned} \mathrm{SL}_k^{\Gamma}[\psi](x) &= \int_{\Gamma} \Phi_k(x,y)\,\psi(y)\,\mathrm{d}s(y)\,, \\ \mathrm{DL}_k^{\Gamma}[\psi](x) &= \int_{\Gamma} \partial_{\nu(y)}\Phi_k(x,y)\,\psi(y)\,\mathrm{d}s(y)\,. \end{aligned}$$

According to Green's representation theorem (see [CoKr13, p. 17]), we have

$$u(x) = \mathrm{SL}_k^{\Gamma}[\partial_\nu u|_{\Gamma}](x) - \mathrm{DL}_k^{\Gamma}[u|_{\Gamma}](x)\,, \qquad x \in D\,. \tag{1.8}$$

Due to the fact that Γ is the disjoint union of Γ_1 and Γ_2, we can rewrite (1.8) as

$$\begin{aligned} u(x) = {} & \mathrm{SL}_k^{\Gamma_1}[\partial_\nu u|_{\Gamma_1}](x) + \mathrm{SL}_k^{\Gamma_2}[\partial_\nu u|_{\Gamma_2}](x) \\ & - \mathrm{DL}_k^{\Gamma_1}[u|_{\Gamma_1}](x) - \mathrm{DL}_k^{\Gamma_2}[u|_{\Gamma_2}](x)\,, \qquad x \in D \end{aligned} \tag{1.9}$$

and similarly we obtain

$$\begin{aligned} v(x) = {} & \mathrm{SL}_{k\sqrt{n}}^{\Gamma_1}[\partial_\nu v|_{\Gamma_1}](x) + \mathrm{SL}_{k\sqrt{n}}^{\Gamma_2}[\partial_\nu v|_{\Gamma_2}](x) \\ & - \mathrm{DL}_{k\sqrt{n}}^{\Gamma_1}[v|_{\Gamma_1}](x) - \mathrm{DL}_{k\sqrt{n}}^{\Gamma_2}[v|_{\Gamma_2}](x)\,, \qquad x \in D\,. \end{aligned} \tag{1.10}$$

By the boundary condition $u|_{\Gamma_2} = v|_{\Gamma_2} = 0$, equations (1.9) and (1.10) can be simplified to

$$u(x) = \mathrm{SL}_k^{\Gamma_1}[\partial_\nu u|_{\Gamma_1}](x) + \mathrm{SL}_k^{\Gamma_2}[\partial_\nu u|_{\Gamma_2}](x) - \mathrm{DL}_k^{\Gamma_1}[u|_{\Gamma_1}](x)\,, \tag{1.11}$$

$$v(x) = \mathrm{SL}_{k\sqrt{n}}^{\Gamma_1}[\partial_\nu v|_{\Gamma_1}](x) + \mathrm{SL}_{k\sqrt{n}}^{\Gamma_2}[\partial_\nu v|_{\Gamma_2}](x) - \mathrm{DL}_{k\sqrt{n}}^{\Gamma_1}[v|_{\Gamma_1}](x)\,, \tag{1.12}$$

where $x \in D$. The boundary integral operators over the surface Γ_i evaluated at a point of Γ_j are defined as

$$\begin{aligned}
\mathrm{S}_k^{\Gamma_i\to\Gamma_j}[\psi|_{\Gamma_i}](x) &= \int_{\Gamma_i} \Phi_k(x,y)\psi(y)\,\mathrm{d}s(y)\,, \quad x\in\Gamma_j\,,\\
\mathrm{K}_k^{\Gamma_i\to\Gamma_j}[\psi|_{\Gamma_i}](x) &= \int_{\Gamma_i} \partial_{\nu_i(y)}\Phi_k(x,y)\psi(y)\,\mathrm{d}s(y)\,, \quad x\in\Gamma_j\,,\\
\mathrm{K}_k^{\top\,\Gamma_i\to\Gamma_j}[\psi|_{\Gamma_i}](x) &= \int_{\Gamma_i} \partial_{\nu_j(x)}\Phi_k(x,y)\psi(y)\,\mathrm{d}s(y)\,, \quad x\in\Gamma_j\,,\\
\mathrm{T}_k^{\Gamma_i\to\Gamma_j}[\psi|_{\Gamma_i}](x) &= \partial_{\nu_j(x)}\int_{\Gamma_i} \partial_{\nu_i(y)}\Phi_k(x,y)\psi(y)\,\mathrm{d}s(y)\,, \quad x\in\Gamma_j\,,
\end{aligned}$$

where $i,j\in\{1,2\}$.

1.3.1 First boundary integral equation

Letting $D\ni x\to x\in\Gamma_1$ in (1.12) and (1.12) and using the jump relations (see [CoKr13, p. 39]), yields

$$u|_{\Gamma_1} = \mathrm{S}_k^{\Gamma_1\to\Gamma_1}[\partial_\nu u|_{\Gamma_1}] + \mathrm{S}_k^{\Gamma_2\to\Gamma_1}[\partial_\nu u|_{\Gamma_2}] - \left(\mathrm{K}_k^{\Gamma_1\to\Gamma_1}[u|_{\Gamma_1}] - \frac{1}{2}u|_{\Gamma_1}\right) \tag{1.13}$$

and

$$v|_{\Gamma_1} = \mathrm{S}_{k\sqrt{n}}^{\Gamma_1\to\Gamma_1}[\partial_\nu v|_{\Gamma_1}] + \mathrm{S}_{k\sqrt{n}}^{\Gamma_2\to\Gamma_1}[\partial_\nu v|_{\Gamma_2}] - \left(\mathrm{K}_{k\sqrt{n}}^{\Gamma_1\to\Gamma_1}[v|_{\Gamma_1}] - \frac{1}{2}v|_{\Gamma_1}\right). \tag{1.14}$$

Taking the difference of (1.13) and (1.14) and using the boundary conditions $u|_{\Gamma_1} = v|_{\Gamma_1}$ and $\partial_\nu u|_{\Gamma_1} = \partial_\nu v|_{\Gamma_1}$, gives the first boundary integral equation

$$\begin{aligned}
0 = &\left(\mathrm{S}_k^{\Gamma_1\to\Gamma_1} - \mathrm{S}_{k\sqrt{n}}^{\Gamma_1\to\Gamma_1}\right)[\partial_\nu u|_{\Gamma_1}] + \mathrm{S}_k^{\Gamma_2\to\Gamma_1}[\partial_\nu u|_{\Gamma_2}]\\
&- \mathrm{S}_{k\sqrt{n}}^{\Gamma_2\to\Gamma_1}[\partial_\nu v|_{\Gamma_2}] - \left(\mathrm{K}_k^{\Gamma_1\to\Gamma_1} - \mathrm{K}_{k\sqrt{n}}^{\Gamma_1\to\Gamma_1}\right)[u|_{\Gamma_1}]\,.
\end{aligned} \tag{1.15}$$

1.3.2 Second boundary integral equation

Applying the same strategy as before for $D\ni x\to x\in\Gamma_2$ in (1.12) and (1.12), yields

$$u|_{\Gamma_2} = \mathrm{S}_k^{\Gamma_1\to\Gamma_2}[\partial_\nu u|_{\Gamma_1}] + \mathrm{S}_k^{\Gamma_2\to\Gamma_2}[\partial_\nu u|_{\Gamma_2}] - \mathrm{K}_k^{\Gamma_1\to\Gamma_2}[u|_{\Gamma_1}] \tag{1.16}$$

and

$$v|_{\Gamma_2} = \mathrm{S}_{k\sqrt{n}}^{\Gamma_1\to\Gamma_2}[\partial_\nu v|_{\Gamma_1}] + \mathrm{S}_{k\sqrt{n}}^{\Gamma_2\to\Gamma_2}[\partial_\nu v|_{\Gamma_2}] - \mathrm{K}_{k\sqrt{n}}^{\Gamma_1\to\Gamma_2}[v|_{\Gamma_1}]\,. \tag{1.17}$$

Taking the difference of (1.16) and (1.17), setting $u|_{\Gamma_2} = v|_{\Gamma_2} = 0$, and applying the boundary conditions $u|_{\Gamma_1} = v|_{\Gamma_1}$ and $\partial_\nu u|_{\Gamma_1} = \partial_\nu v|_{\Gamma_1}$, gives the second boundary integral equation

$$\begin{aligned} 0 = &\left(\mathrm{S}_k^{\Gamma_1\to\Gamma_2} - \mathrm{S}_{k\sqrt{n}}^{\Gamma_1\to\Gamma_2}\right)[\partial_\nu u|_{\Gamma_1}] + \mathrm{S}_k^{\Gamma_2\to\Gamma_2}[\partial_\nu u|_{\Gamma_2}] \\ &- \mathrm{S}_{k\sqrt{n}}^{\Gamma_2\to\Gamma_2}[\partial_\nu v|_{\Gamma_2}] - \left(\mathrm{K}_k^{\Gamma_1\to\Gamma_2} - \mathrm{K}_{k\sqrt{n}}^{\Gamma_1\to\Gamma_2}\right)[u|_{\Gamma_1}]\,. \end{aligned} \tag{1.18}$$

1.3.3 Third boundary integral equation

Next, we apply the normal derivative to (1.12) and (1.12), let $D \ni x \to x \in \Gamma_1$, and use the jump relations. This yields

$$\begin{aligned} \partial_\nu u|_{\Gamma_1} = &\,\mathrm{K}_k^{\top\,\Gamma_1\to\Gamma_1}[\partial_\nu u|_{\Gamma_1}] + \frac{1}{2}\partial_\nu u|_{\Gamma_1} + \mathrm{K}_k^{\top\,\Gamma_2\to\Gamma_1}[\partial_\nu u|_{\Gamma_2}] \\ &- \mathrm{T}_k^{\Gamma_1\to\Gamma_1}[u|_{\Gamma_1}] \end{aligned} \tag{1.19}$$

and

$$\begin{aligned} \partial_\nu v|_{\Gamma_1} = &\,\mathrm{K}_{k\sqrt{n}}^{\top\,\Gamma_1\to\Gamma_1}[\partial_\nu v|_{\Gamma_1}] + \frac{1}{2}\partial_\nu v|_{\Gamma_1} + \mathrm{K}_{k\sqrt{n}}^{\top\,\Gamma_2\to\Gamma_1}[\partial_\nu v|_{\Gamma_2}] \\ &- \mathrm{T}_{k\sqrt{n}}^{\Gamma_1\to\Gamma_1}[v|_{\Gamma_1}]\,. \end{aligned} \tag{1.20}$$

Taking the difference of (1.19) and (1.20) and using the boundary conditions $u|_{\Gamma_1} = v|_{\Gamma_1}$ and $\partial_\nu u|_{\Gamma_1} = \partial_\nu v|_{\Gamma_1}$, gives the third boundary integral equation

$$\begin{aligned} 0 = &\left(\mathrm{K}_k^{\top\,\Gamma_1\to\Gamma_1} - \mathrm{K}_{k\sqrt{n}}^{\top\,\Gamma_1\to\Gamma_1}\right)[\partial_\nu u|_{\Gamma_1}] + \mathrm{K}_k^{\top\,\Gamma_2\to\Gamma_1}[\partial_\nu u|_{\Gamma_2}] \\ &- \mathrm{K}_{k\sqrt{n}}^{\top\,\Gamma_2\to\Gamma_1}[\partial_\nu v|_{\Gamma_2}] - \left(\mathrm{T}_k^{\Gamma_1\to\Gamma_1} - \mathrm{T}_{k\sqrt{n}}^{\Gamma_1\to\Gamma_1}\right)[u|_{\Gamma_1}]\,. \end{aligned} \tag{1.21}$$

1.3.4 Fourth boundary integral equation

Again, we apply the normal derivative to (1.12) and (1.12), let $D \ni x \to x \in \Gamma_2$, and use the jump relations. This gives

$$\begin{aligned} \partial_\nu u|_{\Gamma_2} = &\,\mathrm{K}_k^{\top\,\Gamma_1\to\Gamma_2}[\partial_\nu u|_{\Gamma_1}] + \mathrm{K}_k^{\top\,\Gamma_2\to\Gamma_2}[\partial_\nu u|_{\Gamma_2}] + \frac{1}{2}\partial_\nu u|_{\Gamma_2} \\ &- \mathrm{T}_k^{\Gamma_1\to\Gamma_2}[u|_{\Gamma_1}] \end{aligned} \tag{1.22}$$

and

$$\partial_\nu v|_{\Gamma_2} = \mathrm{K}_{k\sqrt{n}}^{\top\,\Gamma_1\to\Gamma_2}[\partial_\nu v|_{\Gamma_1}] + \mathrm{K}_{k\sqrt{n}}^{\top\,\Gamma_2\to\Gamma_2}[\partial_\nu v|_{\Gamma_2}] + \frac{1}{2}\partial_\nu v|_{\Gamma_2} - \mathrm{T}_{k\sqrt{n}}^{\Gamma_1\to\Gamma_2}[v|_{\Gamma_1}]\,. \tag{1.23}$$

Equations (1.22) and (1.23) can be rewritten as

$$0 = \mathrm{K}_k^{\top\Gamma_1\to\Gamma_2}[\partial_\nu u|_{\Gamma_1}] + \mathrm{K}_k^{\top\Gamma_2\to\Gamma_2}[\partial_\nu u|_{\Gamma_2}] - \mathrm{T}_k^{\Gamma_1\to\Gamma_2}[u|_{\Gamma_1}] - \frac{1}{2}\partial_\nu u|_{\Gamma_2} \tag{1.24}$$

and

$$0 = \mathrm{K}_{k\sqrt{n}}^{\top\,\Gamma_1\to\Gamma_2}[\partial_\nu v|_{\Gamma_1}] + \mathrm{K}_{k\sqrt{n}}^{\top\,\Gamma_2\to\Gamma_2}[\partial_\nu v|_{\Gamma_2}] - \mathrm{T}_{k\sqrt{n}}^{\Gamma_1\to\Gamma_2}[v|_{\Gamma_1}] - \frac{1}{2}\partial_\nu v|_{\Gamma_2} \tag{1.25}$$

respectively. Taking the difference of (1.24) and (1.25) and using the boundary conditions $u|_{\Gamma_1} = v|_{\Gamma_1}$ and $\partial_\nu u|_{\Gamma_1} = \partial_\nu v|_{\Gamma_1}$, gives the fourth boundary integral equation

$$0 = \left(\mathrm{K}_k^{\top\Gamma_1\to\Gamma_2} - \mathrm{K}_{k\sqrt{n}}^{\top\,\Gamma_1\to\Gamma_2}\right)[\partial_\nu u|_{\Gamma_1}] + \mathrm{K}_k^{\top\Gamma_2\to\Gamma_2}[\partial_\nu u|_{\Gamma_2}] - \mathrm{K}_{k\sqrt{n}}^{\top\,\Gamma_2\to\Gamma_2}[\partial_\nu v|_{\Gamma_2}] - \left(\mathrm{T}_k^{\Gamma_1\to\Gamma_2} - \mathrm{T}_{k\sqrt{n}}^{\Gamma_1\to\Gamma_2}\right)[u|_{\Gamma_1}] - \frac{1}{2}\partial_\nu u|_{\Gamma_2} + \frac{1}{2}\partial_\nu v|_{\Gamma_2}\,. \tag{1.26}$$

1.3.5 System of boundary integral equations

The four equations (1.15), (1.18), (1.21), and (1.26) can be written abstractly as

$$Z(k)g = 0 \tag{1.27}$$

with $Z(k)$ given by

$$\begin{pmatrix} \mathrm{S}_k^{\Gamma_1\to\Gamma_1} - \mathrm{S}_{k\sqrt{n}}^{\Gamma_1\to\Gamma_1} & \mathrm{K}_k^{\Gamma_1\to\Gamma_1} - \mathrm{K}_{k\sqrt{n}}^{\Gamma_1\to\Gamma_1} & \mathrm{S}_k^{\Gamma_2\to\Gamma_1} & \mathrm{S}_{k\sqrt{n}}^{\Gamma_2\to\Gamma_1} \\ \mathrm{S}_k^{\Gamma_1\to\Gamma_2} - \mathrm{S}_{k\sqrt{n}}^{\Gamma_1\to\Gamma_2} & \mathrm{K}_k^{\Gamma_1\to\Gamma_2} - \mathrm{K}_{k\sqrt{n}}^{\Gamma_1\to\Gamma_2} & \mathrm{S}_k^{\Gamma_2\to\Gamma_2} & \mathrm{S}_{k\sqrt{n}}^{\Gamma_2\to\Gamma_2} \\ \mathrm{K}_k^{\top\Gamma_1\to\Gamma_1} - \mathrm{K}_{k\sqrt{n}}^{\top\,\Gamma_1\to\Gamma_1} & \mathrm{T}_k^{\Gamma_1\to\Gamma_1} - \mathrm{T}_{k\sqrt{n}}^{\Gamma_1\to\Gamma_1} & \mathrm{K}_k^{\top\Gamma_2\to\Gamma_1} & \mathrm{K}_{k\sqrt{n}}^{\top\,\Gamma_2\to\Gamma_1} \\ \mathrm{K}_k^{\top\Gamma_1\to\Gamma_2} - \mathrm{K}_{k\sqrt{n}}^{\top\,\Gamma_1\to\Gamma_2} & \mathrm{T}_k^{\Gamma_1\to\Gamma_2} - \mathrm{T}_{k\sqrt{n}}^{\Gamma_1\to\Gamma_2} & \mathrm{K}_k^{\top\Gamma_2\to\Gamma_2} - \frac{1}{2}I & \mathrm{K}_{k\sqrt{n}}^{\top\,\Gamma_2\to\Gamma_2} - \frac{1}{2}I \end{pmatrix} \tag{1.28}$$

and

$$g = \begin{pmatrix} \alpha & -\beta & \gamma & -\delta \end{pmatrix}^\top ,$$

where we used the notation

$$\alpha = \partial_\nu u|_{\Gamma_1} , \ \beta = u|_{\Gamma_1} , \ \gamma = \partial_\nu u|_{\Gamma_2} , \text{ and } \delta = \partial_\nu v|_{\Gamma_2} . \tag{1.29}$$

The matrix entries in (1.28) are boundary integral operator with a specific kernel. If the operator O is of the form $\mathrm{O}^{\Gamma_i \to \Gamma_j}$ with $i \neq j$, then the kernel is smooth. Additionally, the kernel of the operator $\mathrm{S}_k^{\Gamma_1 \to \Gamma_1} - \mathrm{S}_{k\sqrt{n}}^{\Gamma_1 \to \Gamma_1}$ is smooth as well. The remaining entries contain a kernel with a weak singularity which is of logarithmic form (notice again that $n \neq 1$ in D). In three dimensions the situation changes slightly to a weak singularity. Hence, in both cases the system can easily be approximated numerically to high accuracy by the boundary element collocation method as developed in [KlLi11, KlLi12] which has been successfully used in [AnChAk13, KiKl12, Kl12b, Kl12c] for the three-dimensional case.

To show that the operator is Fredholm of index zero and analytic for $k \in \mathbb{C} \backslash \mathbb{R}_{\leq 0}$, one would follow the same arguments as given in [Co11, Theorem 5.3.9] or [CoHa13]. The only difficulty is to use the correct Sobolev spaces of the form $\tilde{H}^s(\Gamma_i)$ (see [Mc00] for the definition of the Sobolev spaces) or alternatively the Lions-Magenes spaces $H_{00}^s(\Gamma_i)$ as given in [LiMa72].

1.3.6 Approximation of the system

In this section, we shortly explain how to discretize the resulting boundary integral operator via boundary element collocation method. An extensive explanation has previously been given in [KlLi11, KlLi12] for the three-dimensional case and the two-dimensional case works conceptually similar (see also [At97] for the Laplace equation).

We consider two kinds of scatterers in two dimensions. The first class has a boundary that can be described through polar coordinates and the second class has a boundary that can be described through lines. For the first class, we define the set of points through an equidistant use of the polar angle whereas for the second class the edges are subdivided in equal parts. The curved boundary for the scatterers of the first class is now approximated by a polygon having the previously defined points as vertices. The set of collocation points are the midpoints of each line segment having m collocation points in total. Now, the approximation of each integral over such a line segment can easily be carried out by numerical integration where we assume that the unknown function is approximated by constant interpolation at a midpoint. Note that we have at most a logarithmic singularity in the kernel if the collocation point is situated on a line segment on which we are integrating over. A Gauss-Kronrad quadrature can deal easily with such a singularity.

After the discretization, we can regard (1.28) as a non-linear eigenvalue problem of the form $\mathbf{Z}(k)\tilde{g} = 0$ with $\mathbf{Z}(k) \in \mathbb{C}^{m \times m}$ and $\tilde{g}$ the discretized version

of g given by (1.29) which we solve with Beyn's algorithm [Be12] as done in [CaKr17, Kl13, Kl15, StUn12]. This algorithm uses complex-valued contour integration of the resolvent to reduce the non-linear eigenvalue problem to a linear eigenvalue problem of much smaller size based upon the famous Keldysh's Theorem. For this algorithm one has to specify a 2π-periodic contour in the complex plane and it will find all non-linear eigenvalues situated in this contour to high accuracy due to the fact that the approximation of a 2π-periodic function via the trapezoidal rule yields exponential convergence. We therefore use a circle of radius R with center $C=(c_x,c_y\mathrm{i})$ with $N=40$ nodes for the trapezoidal rule.

1.4 Numerical results

In this section, we present extensive numerical results for some two-dimensional scatterers although we can easily calculate them in three dimensions as shown in [Kl13, Kl15] for the classic interior transmission eigenvalues. The reason is that we can nicely present the corresponding eigenfunctions which is much more difficult in three dimensions.

The first scatterer under consideration is the unit circle $\mathscr{C}$, where we used Γ_1 as the upper half of the circle and Γ_2 as the lower half of the circle. The first five MITEs are given by 1.6818, 2.3185, 2.9533, 3.0791, and 3.1409 where we used the index of refraction $n=4$. After solving the non-linear eigenvalue problem (1.27) using the parameters $N=40$, $R=1/2$, with centers $C=(2,0\mathrm{i})$ and $C=(3,0\mathrm{i})$, respectively, we additionally obtain the discretized version of the functions $\partial_\nu u|_{\Gamma_1}=\partial_\nu v|_{\Gamma_1}$, $u|_{\Gamma_1}=v|_{\Gamma_1}$, $\partial_\nu u|_{\Gamma_2}$, and $\partial_\nu v|_{\Gamma_2}$. We also have $u|_{\Gamma_2}=v|_{\Gamma_2}=0$ and hence we can insert these function approximations into (1.12) and (1.12) in order to compute the approximate solution of u and v at any point situated inside of the scatterer $\mathscr{C}$. We denote with $u^{(i)}$ and $v^{(i)}$ the approximate eigenfunctions corresponding to the i-th MITE. The absolute value of $u^{(i)}$ and $v^{(i)}$ inside $\mathscr{C}$ for the first five MITEs are shown in Fig. 1.2. Note that we were also able to find a complex-valued MITE pair $2.3596+0.3413\mathrm{i}$ and $2.3592-0.34134\mathrm{i}$. The corresponding eigenfunctions $u^{(cv)}$ and $v^{(cv)}$ are also given in Figure 1.2. Since we used constant interpolation for the boundary element collocation method, a linear convergence rate for the eigenvalues is expected and achieved. Note that we do not know the exact MITE values. However, we observe that the error of the imaginary part of the real-valued MITE halves if we double the number of collocation nodes m. In Table 1.1 we clearly see the linear convergence order. Next, we calculate the MITEs for an ellipse $\mathscr{E}$ with major semi-axis 1 and minor semi-axis $4/5$ using the same parameters as before. We obtain the four real-valued MITEs 1.9111, 2.4973, 3.1282, and 3.4609. Additionally, we get the following complex-valued MITE pair $2.7340+0.3801\mathrm{i}$ and $2.7334-0.3802\mathrm{i}$. The corresponding eigenfunctions are shown in Fig. 1.3. If we use the major semi-axis 1 and minor semi-axis $1/2$ for the ellipse with the same parameters as before, we obtain the first four real-valued MITEs 2.7709, 3.1764, 3.7892, and 4.3916. A complex-valued MITE pair is given by $3.8947+0.5352\mathrm{i}$

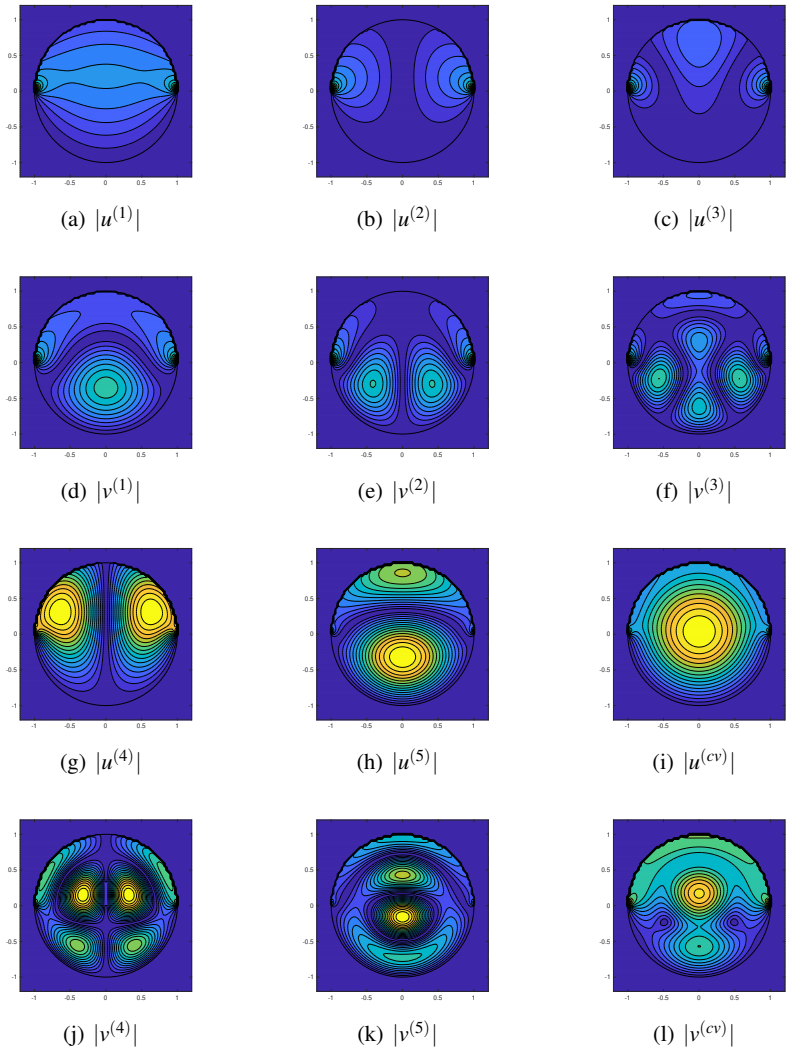

(a) $|u^{(1)}|$ (b) $|u^{(2)}|$ (c) $|u^{(3)}|$

(d) $|v^{(1)}|$ (e) $|v^{(2)}|$ (f) $|v^{(3)}|$

(g) $|u^{(4)}|$ (h) $|u^{(5)}|$ (i) $|u^{(cv)}|$

(j) $|v^{(4)}|$ (k) $|v^{(5)}|$ (l) $|v^{(cv)}|$

Fig. 1.2 The absolute value of the eigenfunctions u (first row and third row) and v (second row and fourth row) for the first five real-valued MITEs and one complex-valued MITE for the unit circle $\mathscr{C}$ using the index of refraction $n = 4$. The MITEs are 1.6818, 2.3185, 2.9533, 3.0791, 3.1409 and $2.3596 + 0.3413$i, respectively.

and $3.8928 - 0.5365$i. Using the minor semi-axis $3/10$ yields the four real-valued MITEs 4.5026, 4.7231, 5.2731, and 5.7279. Note that the classical interior transmission eigenvalues for various minor semi-axis are given in [CaKr17, KlPi18] and a summary of the results for the various ellipses are given in Table 1.2. In Table 1.3 we list the first four real-valued MITEs for deformed ellipses given by the parametriza-

Table 1.1 Convergence of the first five real-valued MITEs for the unit circle C using the index of refraction $n=4$.

m	$k^{(1)}$	$k^{(2)}$	$k^{(3)}$	$k^{(4)}$	$k^{(5)}$
20	$1.6691+0.0445$i	$2.3048+0.0268$i	$2.9405+0.0176$i	$3.1055+0.0063$i	$3.1687+0.0054$i
40	$1.6735+0.0216$i	$2.3075+0.0132$i	$2.9412+0.0094$i	$3.0846+0.0037$i	$3.1475+0.0028$i
80	$1.6772+0.0106$i	$2.3121+0.0066$i	$2.9460+0.0050$i	$3.0800+0.0020$i	$3.1424+0.0014$i
160	$1.6795+0.0052$i	$2.3152+0.0033$i	$2.9495+0.0025$i	$3.0791+0.0010$i	$3.1412+0.0007$i
320	$1.6808+0.0026$i	$2.3170+0.0017$i	$2.9516+0.0013$i	$3.0790+0.0005$i	$3.1410+0.0003$i
640	$1.6814+0.0013$i	$2.3180+0.0008$i	$2.9527+0.0007$i	$3.0791+0.0003$i	$3.1409+0.0002$i
1280	$1.6818+0.0007$i	$2.3185+0.0004$i	$2.9533+0.0003$i	$3.0791+0.0001$i	$3.1409+0.0001$i

Table 1.2 The first four real-valued MITEs for ellipses with major semi-axis 1 and various minor semi-axis using the index of refraction $n=4$.

Minor semi-axis	1st MITE	2nd MITE	3rd MITE	4th MITE
1	1.6818	2.3185	2.9533	3.0791
4/5	1.9111	2.4973	3.1282	3.4609
1/2	2.7709	3.1764	3.7892	4.3916
3/10	4.5026	4.7231	5.2731	5.7279

tion $(3\cos(t)/4+\kappa\cos(2t),\sin(t))$, $t\in[0,2\pi)$ for $\kappa=0,1/10,1/5$, and $3/10$ which has been used before in [CaKr17, KlPi18] for classical interior transmission eigenvalues. We again used $n=4$ and 1280 collocation points and the same boundary conditions as before.

Table 1.3 The first four real-valued MITEs for deformed ellipses with various deformation parameter κ using the index of refraction $n=4$.

κ	1st MITE	2nd MITE	3rd MITE	4th MITE
0	1.9626	2.8575	3.2436	3.6951
1/10	1.9755	2.8404	3.2836	3.6542
1/5	2.0122	2.8087	3.3753	3.5941
3/10	2.0674	2.7899	3.4327	3.6203

The MITEs for the unit square $\mathscr{S}$ using the index of refraction $n=4$ with transmission conditions on the south and east part and homogeneous Dirichlet conditions on the north and west part of the boundary are given by 3.0503, 4.2622, and 5.1805 where we used 512 collocation points and $R=1$ with the centers $C=(2,0\text{i})$, $C=(3,0\text{i})$, and $C=(4,0\text{i})$, respectively. Fig. 1.4 shows the absolute value of the first three eigenfunctions $u^{(i)}$ and $v^{(i)}$ for the unit square. In Fig. 1.5 we display the first three eigenfunctions $u^{(i)}$ and $v^{(i)}$ for the unit square for the eigenvalues 2.6717, 3.6662, and 4.8367, respectively where we used the index of refraction $n=4$ with transmission conditions on the south part and homogeneous Dirichlet condition on the remaining edges. We again used 512 collocation points and $R=1$ with the centers $C=(2.5,0\text{i})$, $C=(3.5,0\text{i})$, and $C=(4.5,0\text{i})$, respectively. Note that in this case it is possible to derive an analytic equation such that its zeros are the MITEs (we refer the reader to Table 1.5 in the Appendix). We obtain with a root finding algorithm

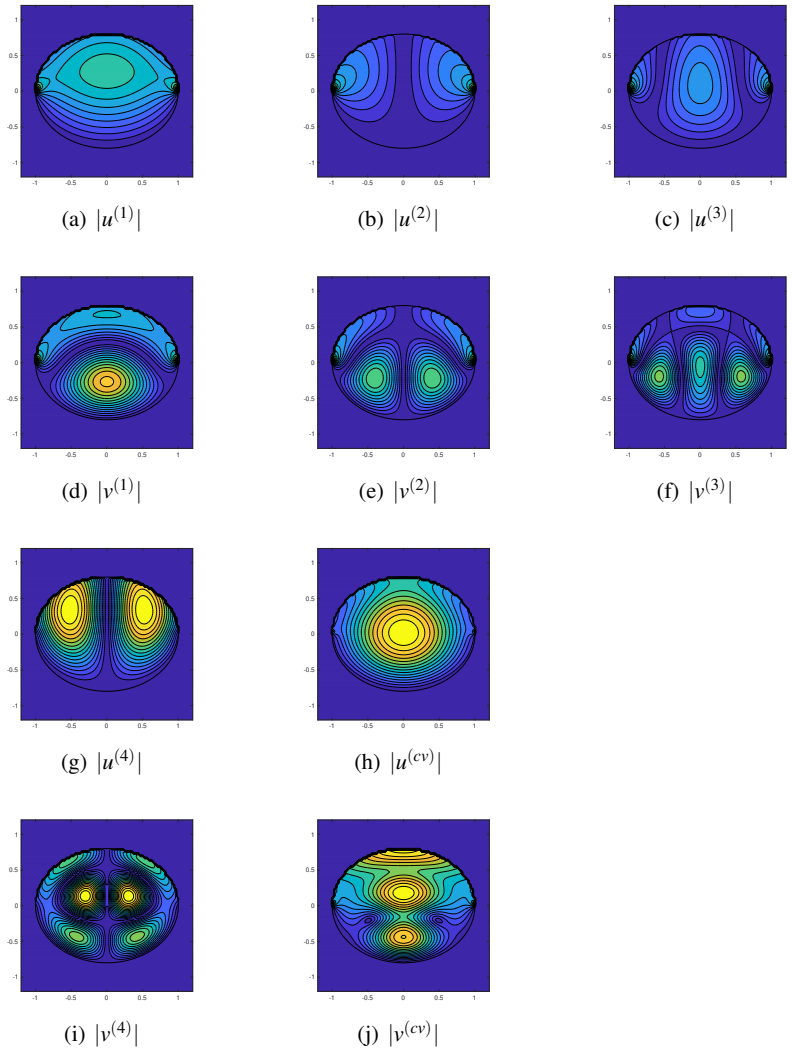

(a) $|u^{(1)}|$ (b) $|u^{(2)}|$ (c) $|u^{(3)}|$

(d) $|v^{(1)}|$ (e) $|v^{(2)}|$ (f) $|v^{(3)}|$

(g) $|u^{(4)}|$ (h) $|u^{(cv)}|$

(i) $|v^{(4)}|$ (j) $|v^{(cv)}|$

Fig. 1.3 The absolute value of the eigenfunctions u (first row and third row) and v (second row and fourth row) for the first four real-valued MITEs and one complex-valued MITE for the ellipse $\mathscr{E}$ using the index of refraction $n = 4$. The MITEs are 1.9111, 2.4973, 3.1282, 3.4609 and $2.7340 + 0.3801\mathrm{i}$, respectively.

2.671 552 787 839 805, 3.666 034 666 514 623, and 4.836 476 632 026 555 and hence the first four digits of the reported results agree.

Next, we also present the first three real-valued MITEs for the unit square where we impose homogeneous Dirichlet condition on the west part and transmission condition on the remaining edges. We use the same parameters as before. We obtain

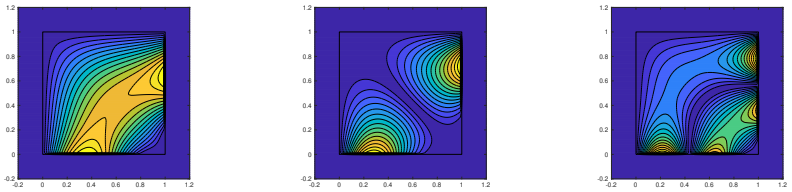

(a) $|u^{(1)}|$ (b) $|u^{(2)}|$ (c) $|u^{(3)}|$

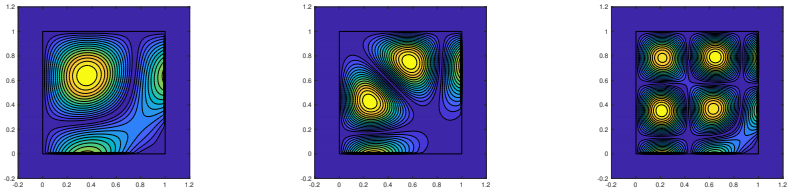

(d) $|v^{(1)}|$ (e) $|v^{(2)}|$ (f) $|v^{(3)}|$

Fig. 1.4 The absolute value of the eigenfunctions u (first row) and v (second row) for the first three real-valued MITEs for the unit square $\mathscr{S}$ using the index of refraction $n = 4$ with transmission conditions on the south and east part and homogeneous Dirichlet conditions on the north and west part of the boundary. The MITEs are 3.0503, 4.2622, and 5.1805, respectively.

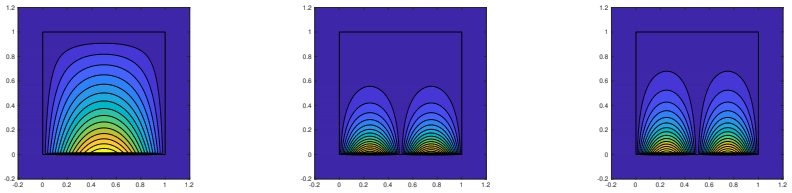

(a) $|u^{(1)}|$ (b) $|u^{(2)}|$ (c) $|u^{(3)}|$

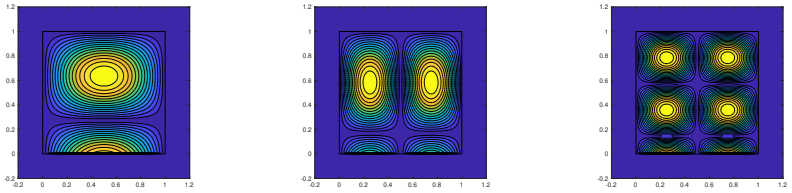

(d) $|v^{(1)}|$ (e) $|v^{(2)}|$ (f) $|v^{(3)}|$

Fig. 1.5 The absolute value of the eigenfunctions u (first row) and v (second row) for the first three real-valued MITEs for the unit square $\mathscr{S}$ using the index of refraction $n = 4$ with transmission conditions on the south part and homogeneous Dirichlet conditions on the remaining edges. The MITEs are 2.6717, 3.6662, and 4.8367, respectively.

4.0802, 5.2285, and 5.7030. The corresponding three eigenfunctions $u^{(i)}$ and $v^{(i)}$ are given in Fig. 1.6.

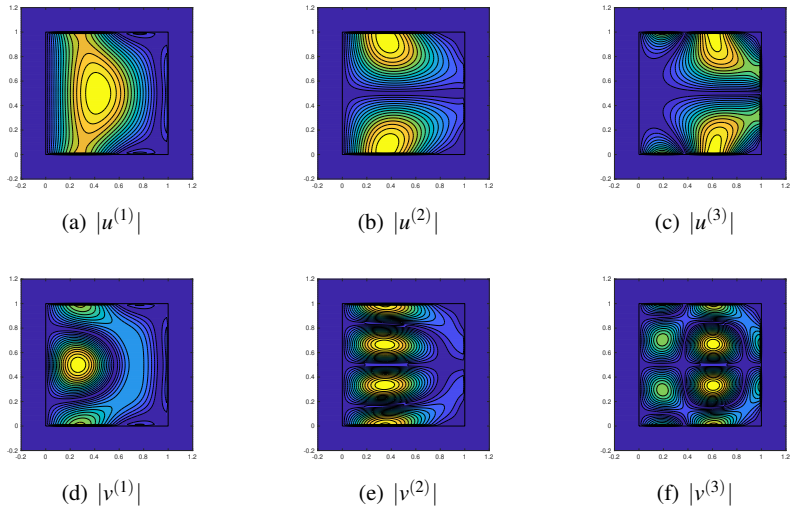

(a) $|u^{(1)}|$ (b) $|u^{(2)}|$ (c) $|u^{(3)}|$

(d) $|v^{(1)}|$ (e) $|v^{(2)}|$ (f) $|v^{(3)}|$

Fig. 1.6 The absolute value of the eigenfunctions u (first row) and v (second row) for the first three real-valued MITEs for the unit square $\mathscr{S}$ using the index of refraction $n = 4$ with homogeneous Dirichlet conditions on the west part and transmission conditions on the remaining edges. The MITEs are 4.0802, 5.2285, and 5.7030, respectively.

To complete our numerical results, we also present numerical results for the case $0 < n < 1$ using the index of refraction $n = 1/2$. Again we use ellipses with various minor axis similar as in Table 1.3. The results are summarized in Table 1.4.

Table 1.4 The first four real-valued MITEs for ellipses with major semi-axis 1 and various minor semi-axis using the index of refraction $n = 1/2$.

Minor semi-axis	1st MITE	2nd MITE	3rd MITE	4th MITE
1	3.1620	4.5193	4.6482	5.8022
4/5	3.5798	4.8518	5.5187	6.2683
1/2	5.1115	6.1186	7.3248	8.4891

To find the MITEs we use a circle with radius $R = 1/2$ and centers $C = (3,0\mathrm{i})$, $C = (4.5,0\mathrm{i})$, and $C = (6,0\mathrm{i})$ in the non-linear eigenvalue solver for the unit circle scatterer whereas we use the centers $C = (3.5,0\mathrm{i})$, $C = (4.5,0\mathrm{i})$, $C = (5.5,0\mathrm{i})$ and $C = (6.5,0\mathrm{i})$ for the ellipse with minor semi-axis $4/5$. For the ellipse with minor semi-axis $1/2$ we use the centers $C = (5,0\mathrm{i})$, $C = (6,0\mathrm{i})$, $C = (7,0\mathrm{i})$ and $C = (8.5,0\mathrm{i})$.

As a final remark, we would like to mention that we also tried different n not satisfying (1.6) and (1.7). In all cases, we have an accumulation point at infinity and

no trouble computing the MITEs. This can also be verified numerically with (1.32) for a variety of n and p.

Additionally, all presented numerical results are indeed mixed interior transmission eigenvalues (not mixed exterior transmission eigenvalues), since we always computed the corresponding eigenfunctions which are zero outside of the domain D. Alternatively, one could impose the additional condition on the far field as done in [CoHa13].

1.5 Summary and conclusion

In this paper, existence and discreteness for mixed interior transmission eigenvalues for a real-valued index of refraction is reviewed and sufficient conditions on the index of refraction as well as the estimates of the lower bound of positive eigenvalues are given. A new system of boundary integral equations to solve the mixed interior transmission problem is derived. Further, it is explained how this system can be approximated via the boundary element collocation method. The resulting non-linear eigenvalue problem is then solved with complex-valued contour integrals. Extensive numerical results for the computation of mixed interior transmission eigenvalues are provided for the first time for a variety of two-dimensional scatterers and might therefore serve as reference values for new algorithms in the future. Further, an explicit expression for mixed interior transmission eigenvalues is given for the unit square and can therefore be used to check the approximation quality of new algorithms. Moreover, the eigenfunctions are shown as well. Hence, it might be worthwhile studying the behavior of the eigenfunctions both for regular scatterers as well as scatterers with corners (see [BlLiLiWa17]). Additionally, a rigorous convergence analysis needs to be worked out in the future. In sum, this chapter might provide a fundamental basis for a further study of this interesting eigenvalue problem. One direction could be the investigation whether the inside-outside-duality method (see [KiLe13, LePe14, PeKl16]) can be applied both theoretically and practically to the mixed interior transmission problem.

Acknowledgements The first author would like to thank the *9th International Conference on Computational and Mathematical Methods in Science and Engineering (CMMSE'19)* steering committee for the opportunity to present the recent results for the numerical calculation of mixed interior transmission eigenvalues on July 2nd, 2019. Further, he would like to thank Christian Constanda for the organization of and the invitation to the special session *Integral Methods in Science and Engineering* at the *CMMSE'19* in Spain. The second author is supported by the National Natural Science Foundation of China (Grant Nos. 91730304 and 11531005).

Appendix

We consider the unit square $\tilde{\square}$ with transmission boundary condition on the north part and homogeneous Dirichlet conditions on the remaining edges. Separation of variables gives

$$\begin{aligned} u(x,y) &= (A\sin(\pi px) + B\cos(\pi px))\left(Ce^{\lambda y} + De^{-\lambda y}\right) \\ v(x,y) &= \left(\hat{A}\sin(\pi px) + \hat{B}\cos(\pi px)\right)\left(\hat{C}e^{\hat{\lambda} y} + \hat{D}e^{-\hat{\lambda} y}\right) \end{aligned}$$

with n the given index of refraction. Here $\lambda = \sqrt{\pi^2 p^2 - k^2}$ and $\hat{\lambda} = \sqrt{\pi^2 p^2 - nk^2}$. Using the boundary condition $u = v = 0$ on the east part yields $B = \hat{B} = 0$, the boundary condition $u = v = 0$ gives $p \in \mathbb{N}$, and the boundary condition $u = v = 0$ on the south part yields $D = -C$ and $\hat{D} = -\hat{C}$. Hence, we have

$$u(x,y) = \sin(\pi px)\left(e^{\lambda y} - e^{-\lambda y}\right), \qquad v(x,y) = c\sin(\pi px)\left(e^{\hat{\lambda} y} - e^{-\hat{\lambda} y}\right)$$

with $c \in \mathbb{R}$ a free parameter. The first transmission condition on the north part ($y = 1$) gives

$$c = \left\{e^{\lambda} - e^{-\lambda}\right\} \setminus \left\{e^{\hat{\lambda}} - e^{-\hat{\lambda}}\right\}. \tag{1.30}$$

The second transmission condition on the north part yields

$$\left(e^{\lambda} + e^{-\lambda}\right)\lambda = c\left(e^{\hat{\lambda}} + e^{-\hat{\lambda}}\right)\hat{\lambda}. \tag{1.31}$$

Inserting (1.30) into (1.31) gives

$$\left(e^{\hat{\lambda}} - e^{-\hat{\lambda}}\right)\left(e^{\lambda} + e^{-\lambda}\right)\lambda - \left(e^{\lambda} - e^{-\lambda}\right)\left(e^{\hat{\lambda}} + e^{-\hat{\lambda}}\right)\hat{\lambda} = 0. \tag{1.32}$$

Hence, the function, say $f_p(k)$, on the right-hand side has to be solved for a given $p \in \mathbb{N}$ with a root finding algorithm in order to obtain the MITE k. Note that the function can be complex-valued and therefore we have to consider separately the real and imaginary part. In Table 1.5 we summarize the highly accurate MITEs using the index of refraction $n = 4$. In parentheses we list the used parameter p.

Table 1.5 The first twelve real-valued MITEs for $\tilde{\square}$ using the index of refraction $n = 4$.

2.671 552 787 839 805 (1)	3.666 034 666 514 623 (2)	4.836 476 632 026 555 (2)
5.037 735 005 038 399 (3)	5.735 963 618 893 019 (1)	5.883 918 727 662 464 (3)
6.294 288 796 613 341 (2)	6.516 005 567 788 862 (4)	7.024 814 731 040 726 (2)
7.038 184 014 872 755 (3)	7.160 899 902 925 930 (4)	7.695 549 983 552 737 (4)

References

[AnChAk13] Anagnostopoulos, K.A., Charalambopoulos, A., and Kleefeld, A.: The factorization method for the acoustic transmission problem. *Inverse Problems*, **29**(11), 115015 (2013).

[At97] Atkinson, K.E.: *The Numerical Solution of Integral Equations of the Second Kind*. Cambridge University Press, Cambridge (1997).

[Be12] Beyn, W.-J.: An integral method for solving nonlinear eigenvalue problems. *Linear Algebra Appl.*, **436**, 3839–3863 (2012).

[BlLiLiWa17] Blåsten, E., Li, X., Liu, H., and Wang, Y.: On vanishing and localizing of transmission eigenfunctions near singular points: a numerical study. *Inverse Problems*, **33**(10), 105001 (2017).

[CaCo06] Cakoni, F. and Colton, D.: *Qualitative Methods in Inverse Scattering Theory - An Introduction*. Springer, Berlin (2006).

[CaCoHa10] Cakoni, F., Colton, C., and Haddar, H.: On the determination of Dirichlet or transmission eigenvalues from far field data. *C. R. Math.*, **348**(7–8), 379–383 (2010).

[CaGiHa10] Cakoni, F., Gintides, D., and Haddar, H.: The existence of an infinite discrete set of transmission eigenvalues. *SIAM J. Math. Anal.*, **42**(1), 237–255 (2010).

[CaKr17] Cakoni, F. and Kress, R.: A boundary integral equation method for the transmission eigenvalue problem. *Appl. Anal.*, **96**(1), 23–38 (2017).

[CoKr13] Colton, D. and Kress, R.: *Inverse acoustic and electromagnetic scattering theory*. Springer, Berlin (2013).

[CoMo87] Colton, D. and Monk, P.: The inverse scattering problem for time-harmonic acoustic waves in a penetrable medium. *Quart. J. Mech. Appl. Math.*, **40**, 189–212 (1987).

[CoMo88] Colton, D. and Monk, P.: The inverse scattering problem for time-harmonic acoustic waves in an inhomogeneous medium. *Quart. J. Mech. Appl. Math.*, **41**, 97–125 (1988).

[Co11] Cossonnière, A.: *Valeurs propres de transmission et leur utilisation dans l'identification d'inclusions à partir de mesures électromagnétiques*. PhD thesis, Université de Toulouse (2011).

[CoHa13] Cossonnière, A. and Haddar. H.: Surface integral formulation of the interior transmission problem *J. Integral Equations Appl.*, **25**(3), 341–376 (2013).

[GiPa13] Gintides, D. and Pallikarakis, N.: A computational method for the inverse transmission eigenvalue problem. *Inverse Problems*, **29**(10), 104010 (2013).

[Ki86] Kirsch, A.: The denseness of the far field patterns for the transmission problem. *IMA J. Appl. Math.*, **37**(3), 213–225 (1986).

[KiGr08] Kirsch, A. and Grinberg, N.: *The Factorization Method for Inverse Problems*. Oxford University Press, Oxford (2008).

[KiKl12] Kirsch, A. and Kleefeld, A.: The factorization method for a conductive boundary condition. *J. Integral Equations Appl.*, **24**(4), 575–601 (2012).

[KiLe13] Kirsch A., and Lechleiter, A.: The inside–outside duality for scattering problems by inhomogeneous media. *Inverse Problems*, **29**(10), 104011 (2013).

[Kl12a] Kleefeld, A.: The exterior problem for the Helmholtz equation with mixed boundary conditions in three dimensions. *Int. J. Comput. Math.*, **89**(17), 2392–2409 (2012).

[Kl12b] Kleefeld, A.: A modified boundary integral equation for solving the exterior Robin problem for the Helmholtz equation in three dimensions. *Appl. Math. Comput.*, **219**(4), 2114–2123 (2012).

[Kl12c] Kleefeld, A.: The transmission problem for the Helmholtz equation in $\mathbb{R}^3$. *Comput. Methods Appl. Math.*, **12**(3), 330–350 (2012).

[Kl13] Kleefeld, A.: A numerical method to compute interior transmission eigenvalues. *Inverse Problems*, **29**(10), 104012 (2013).

[Kl15] Kleefeld, A.: *Numerical methods for acoustic and electromagnetic scattering: Transmission boundary-value problems, interior transmission eigenvalues, and the factorization method*. Habilitation Thesis, Brandenburg University of Technology Cottbus-Senftenberg (2015).

[KlLi11] Kleefeld, A. and Lin, T.-C.: The nonlinear Landweber method applied to an inverse scattering problem for sound-soft obstacles in 3D. *Comput. Phys. Comm.*, **182**(12), 2550–2560 (2011).

[KlLi12] Kleefeld, A. and Lin, T.-C.: Boundary element collocation method for solving the exterior Neumann problem for Helmholtz's equation in three dimensions. *Electron. Trans. Numer. Anal.*, **39**, 113–143 (2012).

[KlPi18] Kleefeld, A. and Pieronek, L.: The method of fundamental solutions for computing acoustic interior transmission eigenvalues. *Inverse Problems*, **34**(3), 035007 (2018).

[LePe14] Lechleiter, A. and Peters, S.: Analytical characterization and numerical approximation of interior eigenvalues for impenetrable scatterers from far fields. Inverse Problems, **30**(4), 045006 (2014).

[LiHuLiLi15] Li, T.-X., Huang, W.-Q., Lin, W.-W., and Liu, J.-J.: On spectral analysis and a novel algorithm for transmission eigenvalue problems. *J. Sci. Comput.*, **64**(1), 83–108 (2015).

[LiLi16] Li, T.-X. and Liu, J.-J.: Transmission eigenvalue problem for inhomogeneous absorbing media with mixed boundary condition. *Sci. China Math.*, **59**(6), 1081–1094 (2016).

[LiMa72] Lions, J.-L. and Magenes, E.: *Non-homogeneous boundary value problems and applications*. Springer, Heidelberg (1972).

[Mc00] McLean, W.: *Strongly elliptic systems and boundary integral operators*. Cambridge University Press, Cambridge (2000).

[PeKl16] Peters, S. and Kleefeld, A.: Numerical computations of interior transmission eigenvalues for scattering objects with cavities. *Inverse Problems*, **32**(4), 045001 (2016).

[StUn12] Steinbach, O. and Unger, G.: Convergence analysis of a Galerkin boundary element method for the Dirichlet Laplacian eigenvalue problem. *SIAM J. Numer. Anal.*, **50**(2):710–728 (2012).

[Su11] Sun, J.: Iterative methods for transmission eigenvalues. *SIAM J. Numer. Anal.*, **49**(5), 1860–1874 (2011).

[YaMo14] Yang, F. and Monk, P.: The interior transmission problem for regions on a conducting surface. *Inverse Problems*, **30**(1), 015007 (2014).

Index